LANGMUIR

Article

pubs.acs.org/Langmuir

Nanoengineered Colloidal Inks for 3D Bioprinting

Charles W. Peak,[†] Jean Stein,[†] Karli A. Gold,[†] and Akhilesh K. Gaharwar*[,†,‡,§]

[†]Biomedical Engineering and [‡]Material Science and Engineering, Dwight Look College of Engineering, and [§]Center for Remote Health Technologies and Systems, Texas A&M University, College Station, Texas 77843, United States

Supporting Information

ABSTRACT: Nanoengineered hydrogels offer the potential to design shear-thinning bioinks for three-dimensional (3D) bioprinting. Here, we have synthesized colloidal bioinks composed of disk-shaped two-dimensional (2D) nanosilicates (Laponite) and poly(ethylene glycol) (PEG). The addition of Laponite reinforces the PEG network and increases viscosity, storage modulus, and network stability. PEG-Laponite hydrogels display shear-thinning and self-recovery characteristics due to rapid internal phase rearrangement. As a result, a range of complex patterns can be printed using PEG-Laponite bioinks. The 3D bioprinted structure has similar mechanical properties compared to the as-casted structure. In addition, encapsulated cells within the PEG-Laponite bioink show high viability after bioprinting. Overall, this study introduces a new class of PEG-Laponite colloidal inks for bioprinting and cell delivery.

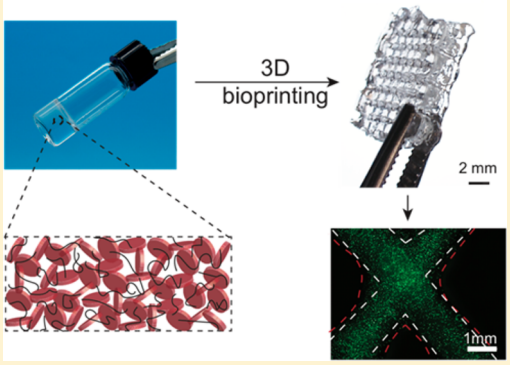

INTRODUCTION

Nanoengineered biomaterials from polymers and nanoclays continue to generate interest in biomedical and biotechnological applications due to their high water content, biocompatibility, and shear-thinning characteristics.[1−3] Swelling clays are layered mineral sheets with isomorphous substitution that results in a permanent positive edge and negative surface charge.[4] Due to the large variation in natural clays, Laponite has become a model system with controllable features during the manufacturing process. Laponite is a two-dimensional (2D) nanomaterial with 30−50 nm in diameter and 1−2 nm in thickness.[5] The hydration of Laponite and internal arrangements result in macroscopic solutions ranging from low viscosity solutions to highly ordered colloidal gels and Wigner glasses.[5] At low salt concentrations ($<10^{-4}$ mM) Laponite (and other clays) remain stable in solution and interact with each other in a "house-of-cards" structure.[6,7] However, with addition of salt, change in pH, or addition of polymer, the phase diagram and subsequent interactions are more difficult to determine. In order to determine precise interactions, various techniques are often used such as dynamic light scattering,[8,9] small angle neutron,[10] or X-ray scattering.[7] Analogous to these techniques is viscosity characterization via shear rheology, which further elucidates the internal structure as macroscopic properties of the material.[11] Additional complexity of Laponite's internal structure occurs with polymer interactions such as gelatin,[12] κ-carrageenan,[13] pluronics,[14−16] poly(*N*-isopropylacrylamide),[17−19] and poly(ethylene oxide)s[11,20−22] due to adsorption/desorption of polymer, additional charge interactions, and ability of both polymer and Laponite to hydrate. Here, we investigate the rheological effect of adsorption/desorption of poly(ethylene glycol) (M_w = 3400 Da) on Laponite at various concentrations and the potential for colloidal suspensions as three-dimensional (3D) printing inks.

Previously Nelson et al. have investigated PEO (−CH_2−CH_2−O−) with low concentrations of Laponite via SANS and DLS measurements[11,22] and rheological work was completed by Schmidt et al. with low concentrations of Laponite.[20,23] Ruzicka et al. have suggested that above the concentration of 3% Laponite, a gel forming structure will result; however, this has not been widely investigated with the addition of polymer chains.[5,24] Earlier work has extensively elucidated the interactions between poly(ethylene glycol/oxide) and Laponite.[11,22,25−27] Quickly desorbing/adsorbing PEG chains onto Laponite changes PEG-Laponite behavior which can be modeled as various fluids such as Newtonian or Bingham Plastic depending on the concentration of each component. Here, we aim to control these interactions for extrusion and bioprinting applications. Colloids show promise for 3D printing applications since they can be precisely tuned to meet various parameters such as shear-thinning and recovery time.

3D printing materials have long been limited to thermoset polymers wherein polymer chemistry dictates their thermoresponsiveness.[28−30] Due to the temperatures at which they must be processed, these polymers often have limited biomedical applications both in their structure and in their ability to extrude living cells. Colloids and hydrogels can overcome the temperature and structure barriers present in current thermoset

Special Issue: Early Career Authors in Fundamental Colloid and Interface Science

Received: July 20, 2017
Revised: October 4, 2017
Published: October 5, 2017

DOI: 10.1021/acs.langmuir.7b02540
Langmuir 2018, 34, 917−925

3D inks. "Bioinks", as they are often named, must be able to support cell viability (cytocompatible), recover quickly for printing, and have cross-linking mechanisms that are compatible with tissues.[31] Hydrogel precursors are often too fluidic to be considered for printing applications and cross-linked hydrogels are too brittle to deform through a needle without fracture. High viscosity colloid systems and nanocomposites fulfill the requirements of a bioink at rest. However, to be a printable system it must first shear-thin followed by a quick rebuilding of internal structure.[32,33] Polymer/clay nanocomposites have previously been demonstrated as shear-thinning.[34−36] As such we further investigate the rheological implications between model clay and polymer system of poly(ethylene glycol) and Laponite for use in 3D bioprinting and cell delivery.

MATERIALS AND EXPERIMENTAL PROCEDURE

Materials. Laponite XLG, procured from Byk Additive and Instruments, was dried in the oven at 100 °C for 4 h to ensure limited environmental water swelling of particles. Poly(ethylene glycol) was dried before acrylate modification using procedures previously reported.[37] In short, 20 g PEG (3.4 kDa) was dissolved in dichloromethane along with triethylamine (Sigma). Acryloyl chloride (Alfa Aesar) was added dropwise to the solution on ice and stirred for 24 h. After washing, the solution was precipitated into diethyl ether and dried over vacuum. ^{1}H NMR (300 MHz, $CDCl_3$, δ): 3.62 (s, 297H; $-OCH_2CH_2$), 5.81 (dd, 2H, J = 10.5 and 1.2 Hz; $-CH{=}CH_2$), 6.40 (dd, 2H, J = 17.3 and 1.5 Hz; $-CH{=}CH_2$) confirmed diacrylation of PEG3.4 kDa.

Synthesis of PEG-Laponite Colloids. The desired amounts of clay and PEGDA were dispersed into 18 MΩ water (pH = 7.4) and vortexed vigorously for at least 2 min. For rheological time sweeps, samples were immediately loaded and tested. For all other experiments, the solutions were allowed to sit for 24 h before use as determined by the initial time sweep. Samples were carefully loaded onto a Peltier plate base as to not disrupt internal structure formation. Once geometry was lowered, samples were allowed 15 min to equilibrate.

Rheological and Mechanical Characterization. A Discovery Hybrid Rheometer 2 (DHR-2) (TA Instruments) with attached 40 mm parallel plate at gap height of 0.25 mm and 25 °C for all experiments. Precursor solutions of PEG and PEG/XLG were used for all experiments unless otherwise noted. Rotational time sweeps were executed for 18 h at 1 Pa, 1 Hz to determine aging time and dynamics of solutions. Rotational shear rate sweeps were executed between 10^{-6} and 10^3 (s^{-1}) to determine the yield stress and the power law region. Power-law parameter n (flow behavior index) was calculated using TRIOS software (TA Instruments). Rotational time sweeps were executed at three different shear rates (s^{-1}) in sequential order: 10^{-2} (60 s), 3000 (5 s), 10^{-2} (120 s) to determine shear recovery of solutions. Time to 80% recovery was manually observed/calculated.[32] Oscillatory shear stress sweeps between 10^{-1} and 10^3 were performed at 1 Hz and frequency sweeps between 10^{-2} and 10^2 were performed at 10 Pa to further validate yield points and investigate dependence on frequency. Increasing stress was applied to the samples (1, 10, 50, 100, 300, 500, 1000 Pa) and storage modulus was monitored to further verify yield stress. Creep experiments were conducted by applying 50 Pa stress for 5 min followed by 15 min of recovery (no applied stress). Data from creep experiments were evaluated by attempted fitting of the creep region with the Burger model

$$J_c(t) = J_0 + J_1\left[1 - \exp\left(-\frac{t}{\tau}\right)\right] + t/\eta$$

$J_c(t)$ is the compliance of samples measured by the instrument at time t. J_0 is the instantaneous compliance and J_1 is the retarded compliance corresponding to Maxwell and Kelvin−Voigt elements, respectively. τ is the retardation time and η is the Newtonian viscosity. Ultraviolet curing of samples at 7 mW/cm^2 occurred, and subsequent oscillatory frequency and stress sweeps as described above were conducted on cured hydrogel samples. An ADMET eXpert 7600 Single Column Testing System equipped with 25 lb load cell was used for compression testing of 3D printed and cast (bulk) hydrogel. Strain rate of 1 mm/min was used to compress the samples 50% of original height. The compressive modulus was calculated and plotted to compare bulk versus 3D printed structures. Print fidelity was calculated as

$$\left(\frac{\text{Actual Print}}{\text{Programmed Print}} - 1\right) \times 100$$

In Vitro Studies. Murine preosteoblasts (NIH MC3T3 E1−4, ATCC) were grown in alpha modified MEM (Hyclone, GE Lifesciences), supplement with 10% fetal bovine serum, and passaged at 80% confluency. Passages 4−6 were used for all experiments. After passaging, counting was completed and cells were resuspended and aliquoted into Eppendorf tubes at 10,000 cells per mL solution. Solutions were gently pipetted or mixed to achieve a homogeneous cell distribution. To visualize cells encapsulated within bioinks, cells were incubated at 37 °C with 2 μM Cell Tracker Green Dye (ThermoFisher) in 1× PBS for 30 min prior to passaging. Cell imaging was performed using a (SteREO Discovery v 8, Carl Zeiss) microscope after extrusion. Images were processed and analyzed in ImageJ (NIH) to quantify localization of extruded samples.

3D Printing. PEG-Laponite constructs were fabricated utilizing a HYREL System 30 M 3D printer. The PEG-Laponite colloid was loaded into a HYREL VOL-25 extruder (HYREL L.L.C., Norcross, GA) equipped with a luer lock adapter and 23 gauge, 5-mm-long blunted stainless steel needle (Jensen Global Inc., Santa Barbara, CA). Once connected to the printer, constructs were modeled in Solidworks 3D CAD Design, exported as an STL file, and imported into Slic3r version 1.2.9. Overall, this process converts the Solidworks design into layer-by-layer instructions for the printer, or G-code. The G-code files are then imported into HYREL's proprietary software (Repetrel Rev 2.828) and printed at room temperature onto glass slides. Upon completion, glass slides were placed under a UV lamp and photo-cross-linked for 150 s at an intensity of 7 mW/cm^2.

Statistical Methods. The data is presented as the means ± standard deviations of the experiments (n = 3−5). Statistical analysis was performed via one-way ANOVA with posthoc Tukey's test using GraphPad Prism (v 6.01). Levels of significance were assigned as * = p < 0.05, ** = p < 0.005, *** = p < 0.0005, and **** = p < 0.0001.

RESULTS AND DISCUSSION

Colloidal Bioink Synthesis. Laponite XLG has a complex phase diagram that ranges from sols and gels.[5] Being a synthetic clay, the production process of Laponite precisely controls its size, shape, and chemical makeup; therefore, it has been used as a model clay system. However, several groups continue to investigate various aspects of Laponite exfoliation, nematic order, and structure through means such as dynamic light scattering,[11] rheology,[20] and SANS/SAXS.[14,22] The addition of polymer, regardless of molecular weight, results in ongoing adsorption and desorption of polymer to clay platelets which may alter the phase diagram boundaries of Laponite. We aim to use the reported internal "house-of-cards" structure of Laponite as a suitable matrix for 3D printing.[5] Gel forming solutions of poly(ethylene glycol) (10% wt./vol, 3.4 kDa) occurred with concentrations above 4% Laponite after 24 h. Over longer periods of time (months), solutions containing 2% Laponite will form a gel but can easily be disturbed and liquefy, and subsequently must undergo aging once more. Laponite XLG form a "house-of-cards" structure upon exfoliation or hydration of particles.[6,24] This internal structure has been previously studied via dynamic light scattering.[38] The buildup of structure

DOI: 10.1021/acs.langmuir.7b02540
Langmuir 2018, 34, 917−925

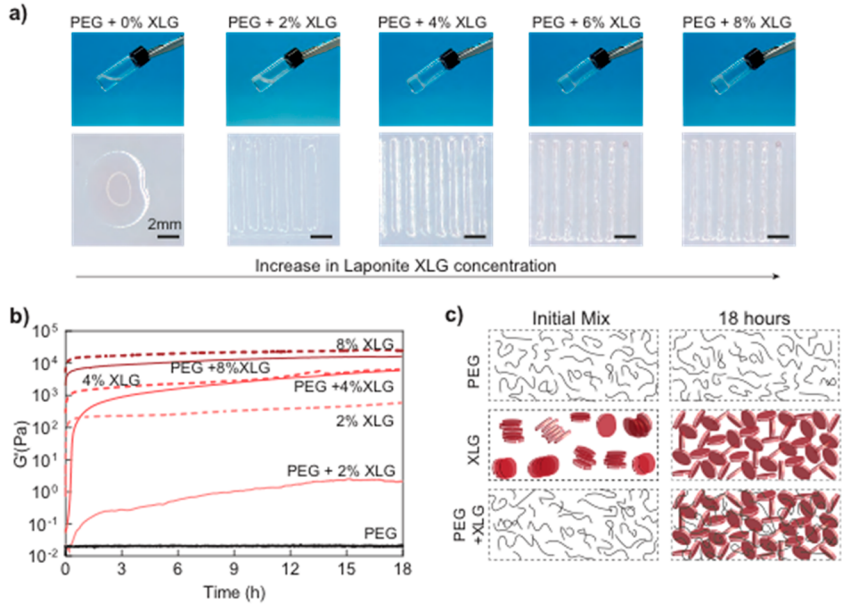

Figure 1. Synthesis of PEG-Laponite colloidal solution. (a) Viscosity increases at rest with increasing Laponite XLG concentration; changes in print quality with increase of Laponite XLG concentration; (b) time sweep of solutions of PEG/Laponite, PEG, and Laponite; (c) schematic of internal structure formation of PEG, Laponite, and PEG/Laponite solutions.

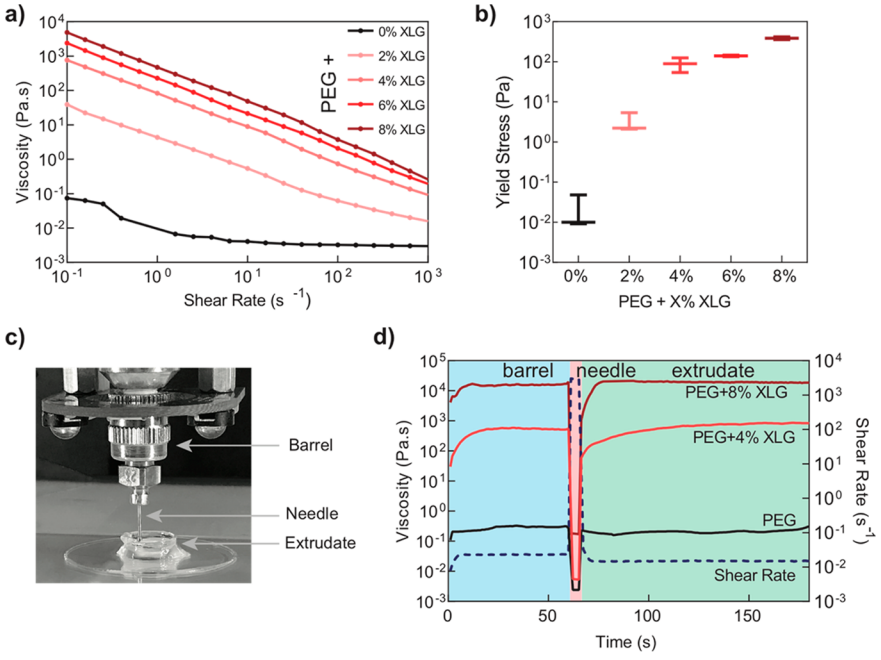

Figure 2. Laponite induces shear-thinning characteristics to PEG solution. (a) shear rate sweep of PEG/Laponites suspensions; (b) yield stress quantification of PEG/Laponite concentrations; (c) illustration of extrusion through a syringe barrel, needle, and onto print-bed; (d) peak hold experiments to mimic flow during extrusion/printing.

resulted in an increase in solution viscosity which can be useful for three-dimensional printing applications (Figure 1a). Time sweeps (1 Hz, 1 Pa) indicated that there is a delay in PEG-Laponite XLG gel formation at initial time points as indicative of increasing storage modulus (Figure 1b). This may be due to competition between Laponite and PEG becoming fully hydrated or rapid adsorption and desorption of PEG to the Laponite particles.[27] Samples containing 6% Laponite were removed for graph clarity. At longer time points (18+ h) the shear storage modulus (G') was concentration dependent based on how much space was filled within the solution and by how much water adsorbed to the surface of the Laponite. PEG concentration was kept constant at 10% wt/vol while Laponite XLG concentration was varied. Here we observed that PEG solutions containing 2% wt/vol Laponite XLG did not form a strong internal structure after 18 h. In addition, at any given concentration of Laponite XLG, the addition of PEG either decreased the storage modulus or increased the time for storage modulus plateau to occur. Nuclear magnetic resonance spectroscopy (NMR) analysis by Lorthioir et al. suggests that PEG/Laponite systems are dynamic yet have strong local constraints that slow down segmental motions of the PEG

DOI: 10.1021/acs.langmuir.7b02540
Langmuir 2018, 34, 917−925

Table 1. Summary of Power-Law Parameters for PEG/Laponite XLG Solutions

	PEG (10% wt/vol) + *X*% (wt/vol) Laponite XLG				
	0	2	4	6	8
n	0.96 ± 0.02	0.22 ± 0.10	0.20 ± 0.16	0.22 ± 0.27	0.29 ± 0.05
K	0.0029 ± 0.0003	6 ± 1	60 ± 34	149 ± 24	169 ± 43

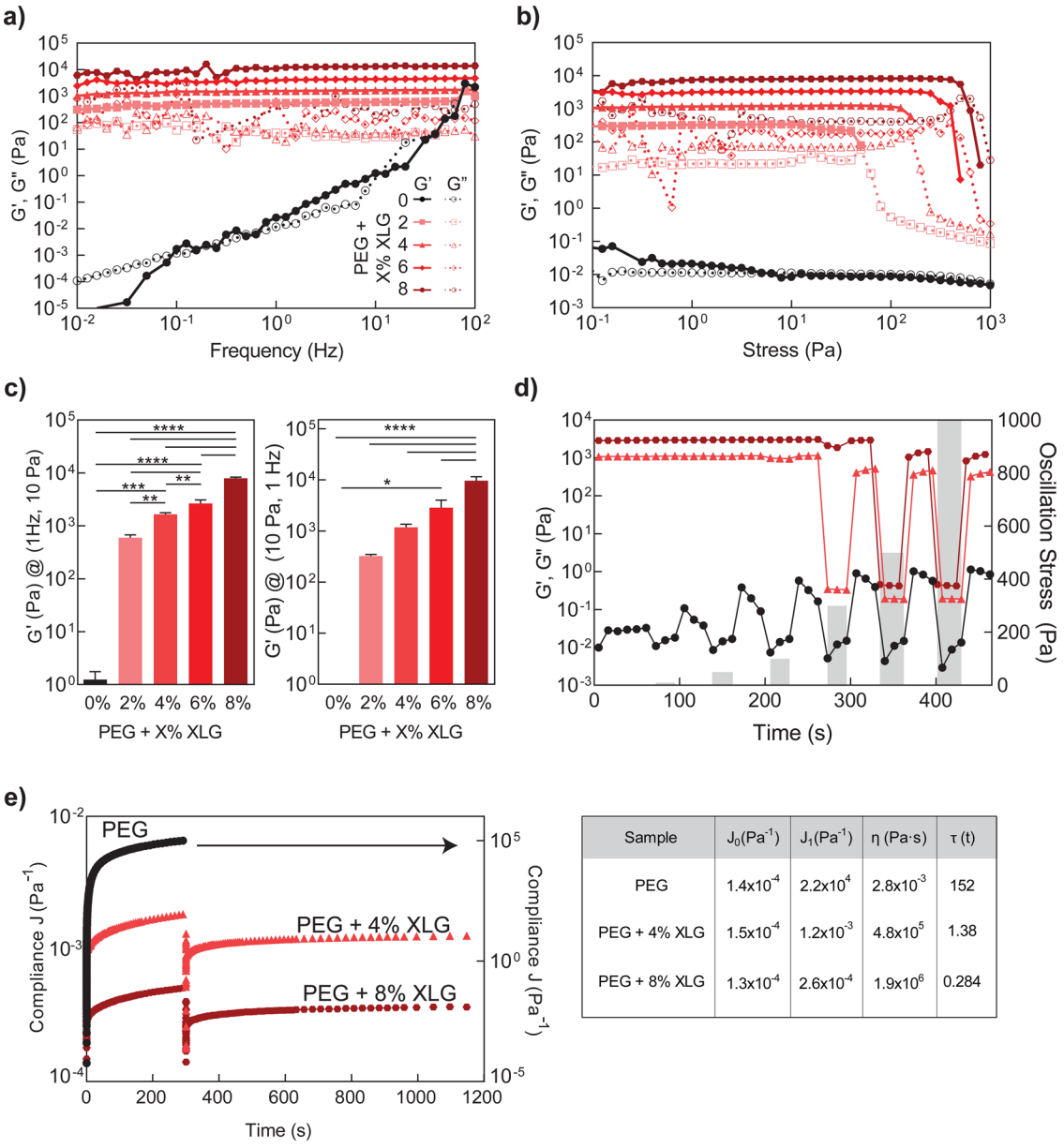

Sample	J_0(Pa^{-1})	J_1(Pa^{-1})	η (Pa·s)	τ (t)
PEG	1.4×10^{-4}	2.2×10^{4}	2.8×10^{-3}	152
PEG + 4% XLG	1.5×10^{-4}	1.2×10^{-3}	4.8×10^{5}	1.38
PEG + 8% XLG	1.3×10^{-4}	2.6×10^{-4}	1.9×10^{6}	0.284

Figure 3. Rheological sweeps of un-cross-linked PEG/Laponite suspensions (a) Frequency sweeps from 10^{-2} to 10^{2} Hz; (b) stress sweeps from 10^{-1} to 10^{3} Pa; (c) storage modulus at 1 Hz from samples; storage modulus at 10 Pa from samples. For all data, * indicates $p < 0.05$, ** $p < 0.005$, *** $p < 0.0005$, **** $p < 0.0001$. (d) Increasing applied stress with monitored storage modulus. (e) Representative creep and recovery curves for PEG/Laponite solutions. PEG plotted on right *y*-axis (as indicated by arrow), PEG/4% and 8% are plotted on left *y*-axis.

backbone[27] suggesting that the observed decrease in storage modulus is most likely due to intermolecular motions of PEG adsorbing/desorbing from the surface of Laponite XLG. Solutions seemingly underwent a shift from tactoid sheets and random polymer configuration to a disconnected "house-of-cards" with PEG adsorbed on the surface (Figure 1c). Particles underwent what is known as jamming transition during which movement is restricted since there is no physical space within the solution, thus lowering the amount of free energy required to remain in suspension.[25,26,39] A flocculation was avoided by balancing the colloid electrostatic repulsions and attractive van der Waals forces.[40]

Addition of Laponite to PEG Results in Shear-Thinning Bioink. After the time-aging of solutions occurred, the solutions were still able to flow with an applied stress or an induced shear rate.[20] Subsequently, the solution was broken down with an increase in shear rate (Figure 2a). Previous studies suggest that there are two flow regions of Laponite with

DOI: 10.1021/acs.langmuir.7b02540
Langmuir 2018, 34, 917−925

an induced shear rate: plug-like flow and Newtonian-like flow.[41] During and after the transition of flow types, it is suggested that the internal network is broken into smaller blocks that freely move as solid bodies within a fluidic matrix. Thus, PEG/Laponite XLG materials must overcome a yield stress before they can be smoothly extruded or printed (Figure 2b). Several fluid models can be used to describe PEG/Laponite XLG systems such as Herschel-Bulkley model or shear-thinning model. During printing application, shear-rate is determined according to eq 1

$$\dot{\gamma} = \frac{3n+1}{4n} \times \frac{4Q}{\pi R^3} \quad (1)$$

where n is the shear-thinning index, Q is the volumetric flow rate, and R is the radius of the annulus. It was determined that shear-rates experienced in typical printing parameters (Q = 300 μL/min, R = radius of gauged needle) are between 10^{-1} and 10^3 s^{-1}. The shear-thinning index is determined by power law fitting of the viscosity vs shear rate curve as described in eq 2

$$\eta = K\dot{\gamma}^{n-1} \quad (2)$$

where η is viscosity, K is the flow consistency index (defined as the viscosity when shear-rate is 1 s^{-1}), and n is the shear-thinning index. Table 1 summarizes the K and n values.

Addition of Laponite XLG decreased n due to disruption of the balance between the van der Waals and electrostatic forces. K increased due to a close packed "house-of-cards" structure where the repulsion forces are balanced with attractive forces. There was a denser packed "house-of-cards" (edge to face platelet orientation) internal structure[42] of samples containing 6% and 8% Laponite XLG when compared to 2% and 4% containing samples, which resulted in an overall increase in viscosity across all shear rates (Figure 2a). The power law index can describe the degree of shear-thinning a solution exhibits. When n = 1, the solution is Newtonian; n < 1 shear-thinning; n > 1 shear thickening. With any addition of Laponite there was a significant decrease in n compared to PEG solutions, suggesting that Laponite is the cause of shear-thinning. With an induced shear, Laponite orients itself parallel to the direction of flow.[20] It is suggested that due to electrostatic charge, two parallel Laponite particles repel each other therefore gliding over each other to produce a shear-thinning fluid. While numerical values are not significantly different, it is hypothesized that larger or more numerous sections of the PEG/4−8% Laponite solutions are flowing within the medium and have not fully broken up.[41] Previous work has analyzed shear-induced flow of clay nanoparticles (3% wt/vol), supporting a decrease in viscosity with an increase in shear rate.[20,41−43]

Injection and extrusion based direct-write 3D printing materials must first meet the criteria for shear-thinning, which describes the change from soft-solid/gel to fluid/low viscosity (η < 100 Pa.s). Once material has exited the end of the deposition needle, rebuilding time of the internal structure can predict the amount of localization versus spreading and its ability to be used in 3D printing. As such, unidirectional flow through a syringe and needle (Figure 2c) were modeled using rheometry (Figure 2d). Rheometry was used to quantify the solution's "printability" by observing the change in viscosity with a change in shear rate. During initial stages, solutions are in a barrel and experience low shear rate ($\dot{\gamma}$ < 1 s^{-1}). Once solutions enter the needle shear-rates increase to upward of 10^2−10^4 s^{-1} depending on volumetric flow rate. Once exited, the flow stops and the material must quickly regain viscosity—viscosities above ~10^2 Pa.s were desirable as they have previously been reported as printable.[44,45] The viscosity change over time, induced by changes in shear rate (Figure 2d), can indicate how quickly a solution rebuilds (thixotropy) thereby elucidating its usefulness as an ink. PEG behaved as a fluid across all shear rates and variation in the viscosity measurement was attributed to surface tension between solution and the upper geometry. Solutions containing Laponite XLG underwent rapid breakdown and rebuild. Recovery of 80% of initial viscosity was considered significant. Increasing Laponite XLG concentrations decreased the recovery time due to incomplete destruction of internal "house-of-cards" structure (Figure S2). In solutions containing greater concentrations of Laponite XLG, larger sections of polymer/clay mixture exist and therefore can quickly agglomerate compared to 4% containing samples. Balance between solution yield stress, ability to shear-thin, and structure rebuilding must be optimized for injection and printing applications.

Laponite Increase Mechanical Stability of Colloidal Bioink. PEG/Laponite XLG mixtures can be described both as highly viscous fluids and as soft solids. As such, we continued investigating via oscillatory rheometry with stress and frequency sweeps to determine shear storage modulus (G') and any dependency on stress or frequency of un-cross-linked samples. PEG behaved as a Newtonian fluid with an increase in applied frequency (Figure 3a). With an increase in frequency, the storage modulus increased as the PEG solution responded to increasing frequency. Formation of an internal structure via the addition of Laponite XLG negated all frequency dependencies of the fluid. Increased storage modulus was observed and attributed to an increase in fill volume/decrease of free space for water movement. Increasing Laponite XLG concentration increased G' in a similar fashion to the increased viscosity. Further, frequency sweeps were used to determine the linear viscoelastic region for samples. Stress sweeps (Figure 3b) were used to verify trends in yield point (though yield point was determined via rotational tests as previously discussed). Oscillatory stress sweeps resulted in crossover points (G' < G'') of 6.48 ± 2.07, 35.25 ± 17.56, 147.61 ± 18.82, 297.13 ± 79.62, and 544.37 ± 74.89 Pa for samples that contained 0, 2, 4, 6, and 8% Laponite, respectively. Again, with increasing concentrations of Laponite XLG an increase in storage modulus was presented. Solutions with 8% wt/vol Laponite were statistically significant (p < 0.0001) compared to all other compositions for both frequency and stress sweeps (Figure 3c). As further verification of yield stress, an increasing amount of stress was applied to un-cross-linked PEG/Laponite samples (Figure 3d). Rapid breakdown of structure occurred once applied stress was above the yield stress. Storage modulus recovery for PEG solutions was nonexistent while PEG/4% Laponite solutions recovered 50.3% of storage modulus and PEG/8% Laponite solutions recovered 58.7% of the storage modulus. Storage modulus remained >500 Pa for all recovered samples. The effect of Laponite on the viscoelastic properties of PEG precursor solutions is most evident through creep experiments. By fitting the creep curves of samples with Burger's model,[46] J_0, J_1, τ, and η were obtained (Figure 3e). Representative creep curves highlight the recovery for samples containing Laponite XLG as compared to PEG. The PEG compliance curve showed high compliance but no recovery. Compliance is inversely proportional to modulus which corroborated data presented in Figure 3a,b. Samples of PEG/4% and 8% Laponite XLG exhibited recovery due to possible

DOI: 10.1021/acs.langmuir.7b02540
Langmuir 2018, 34, 917−925

polymer bridging of Laponite XLG particles which are able to store accumulated strain in the sample and then release as elastic recovery upon relaxation (cessation of applied stress).[47] Storage modulus and viscosity both indicate if a material can support itself without external support material. In particular, viscosity recovery after shear dictates the ease of incorporating cells for use as bioinks. Quick material recovery suggests that incorporation of cells may need to be pipetted multiple times. As such, 4% Laponite XLG samples were chosen for printing applications as it balances the viscosity recovery and storage modulus.

3D Bioprinting Using Colloidal Bioinks. Localization of cells and therapeutics is of utmost importance for biomedical applications. Within literature, shear-thinning has been the focus of printing applications as it will dictate a material's ability to flow through a needle.[48−51] Once the material has exited the needle the shear forces placed on the material cease and recovery (Figure 2d) will indicate final placement of extrudate compared to the material's ability to shear-thin. Therefore, the materials we developed have the potential for printing applications. To demonstrate bioprinting applications, murine preosteoblasts were incorporated into PEG/4% Laponite and printed to create a circle and crosshatch shapes (Figure 4a,b). Printed constructs of PEG/4% Laponite achieved heights up to 23 layers tall without support material or collapse. Low amounts of spreading occurred for PEG/4%Laponite solutions as predicted through the peak hold tests (Figure 2d).

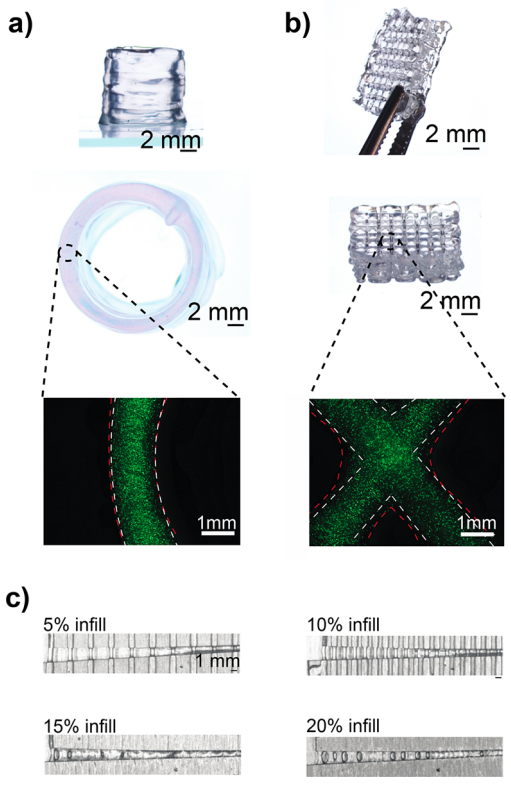

Figure 4. Bioprinting of colloidal inks. (a) 3D printed circle of PEG/4% Laponite with preosteoblasts and cell tracker images (b) 3D printed crosshatch structure of PEG/4% Laponite with preosteoblasts and cell tracker images. Note: For both (a) and (b) white dashed lines represent the programed print path and red dashed lines represent the 3D printed contruct. (c) PEG/4% Laponite bridging gaps up to 2.5 mm.

Localization of cell delivery occurred with PEG/4% Laponite samples compared to PEG and phosphate buffered saline solution (PBS) samples as measured via cell tracker experiments (Figure S3). The amount of spreading (print fidelity) as indicated by the separation of the red and white lines indicate that PEG/4% Laponite samples have more precise local delivery and shorter recovery time compared to PEG or PBS. There was a statistically significant difference ($p < 0.0001$) between PBS and PEG/4% Laponite printed structures as well as between PEG and PEG/4% Laponite in terms of print fidelity. PEG/4% Laponite resulted in structures 7 ± 19% larger than designed while PEG structures spread 413 ± 76% and PBS spread 376 ± 47%. The lack of spreading permitted PEG/4% Laponite bridging a gap of 2.5 mm across a variety (5−20%) of infill density (Figure 4c). While PEG/6% and 8% Laponite samples have higher storage modulus (Figure 3c) and viscosity (Figure 2a), inhomogeneous incorporation of cells was observed due to high yield stress and quick recovery times. As cells were added to the solution, they were unable to flow within the solution as it presented itself as a solid object rather than a viscous colloid. For PEG/4% Laponite, live/dead (Figure S4) indicated that across several volumetric flow rates (500, 1000, 2000 μL/min) there was no difference in viability immediately post injection. Two-dimensional seeding of preosteoblasts on PEG/Laponite hydrogels and subsequent proliferation have previously been reported.[52−55] In addition, long-term cell viability, up to 3 weeks, within PEG-based hydrogels has been demonstrated with osteoblasts, chondrocytes, HUVECs, and β-cells in previous studies.[56−59] To facilitate long-term cell viability, the macroporous structure can be controlled through changing the density of the crosshatch layer, as demonstrated in Figure 4b, aiding nutrient administration and waste removal. Printing of solutions is a macroscopic physical representation of the rheological properties of un-cross-linked solutions. Printed structures exhibited low sagging and precision in deposition. Cell tracker and live/dead images coupled with printing images indicated that PEG/Laponite rheological properties meet the requirements necessary for bioprinting.

Covalently Cross-Linked Colloidal Bioinks. In the 3D printing process, the un-cross-linked hydrogel is extruded until print completion and subsequently exposed to ultraviolet light for cross-linking to occur. 3D printed structures using colloidal bioink showed high mechanical stiffness and could sustain mechanical deformation (Figure 5a). Compressive modulus of print and cast hydrogels were compared and no difference was observed as determined with a Student's t test. Printed structures may develop anisotropy due to particle alignment.[60] However, anisotropy was observed in PEG/Laponite, suggesting that the internal "house-of-cards" Laponite structure was conserved during extrusion. Oscillatory shear experiments of cross-linked hydrogels were used to determine viscoelastic properties. Hydrogels were UV cross-linked and subjected to oscillatory shear stress (1 Hz) and frequency sweep (1 Pa) experiments, and the materials' response in terms of elastic moduli (G') and viscous moduli (G'') were measured. All hydrogels were found to have a large viscoelastic plateau within the range measured. Interestingly, PEG hydrogels were not dependent on frequency (Figure 5b) compared to un-cross-linked samples (Figure 3a). Prior to UV cross-linking an internal network was not present within PEG, after UV cross-linking covalent bonds are formed between PEG chains, therefore storing energy put into the system. Covalent bonds

DOI: 10.1021/acs.langmuir.7b02540
Langmuir 2018, 34, 917−925

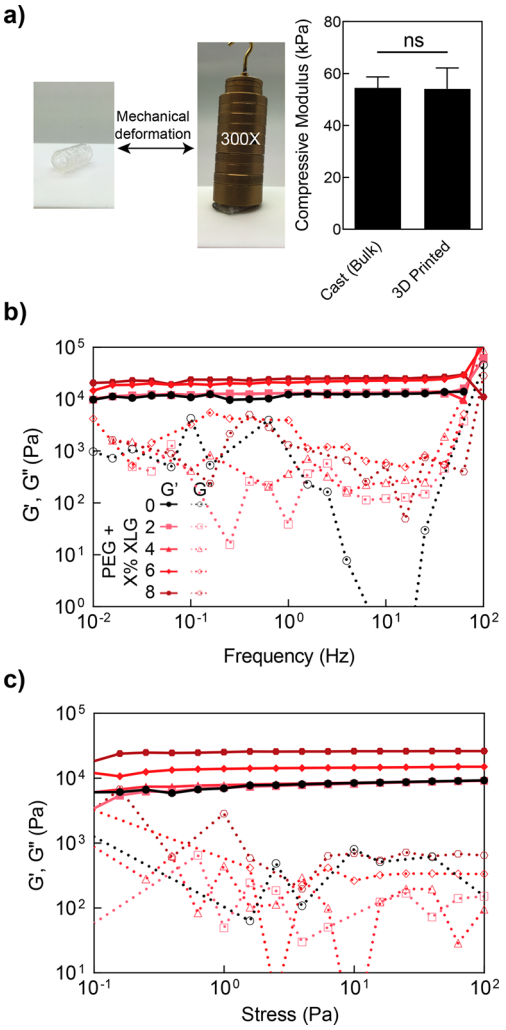

Figure 5. Covalently cross-linked PEG-Laponite network. (a) Covalently cross-linked 3D printed structure using PEG/Laponite bioink shows high mechanical stiffness and elasticity. Compressive modulus of PEG/4% Laponite for cast and 3D printed constructs. Rheological sweeps of cross-linked PEG/Laponite suspensions. (b) Frequency sweeps from 10^{-2} to 10^{2} Hz; (c) stress sweeps from 10^{-1} to 10^{3} Pa.

require more energy to break compared to electrostatic attractive forces that dominate in un-cross-linked samples leading to stability across frequency and stress ranges. Internal structure was not broken down within cross-linked hydrogels during a stress sweep; however, it is noted that the viscous modulus (G'') is highly variable suggesting internal rearrangement of polymer and Laponite structure. Further stress sweep experiments (Figure 5c) suggested that upon cross-linking the samples do not mechanically yield within the experimental range and there is no decrease in storage modulus. Again, the presence of covalent cross-linking prevented yielding of the material as covalent bonds are much stronger compared to weak electrostatic interactions occurring in un-cross-linked colloids. These results, when coupled with the un-cross-linked flow parameters, suggest that PEG/Laponite samples are effective both in extrusion/printing applications and as a stable matrix once cross-linked.

CONCLUSIONS

This study has investigated the rheological modification of PEG precursor solutions via incorporation of Laponite XLG clay nanoparticles. PEG/Laponite XLG form internal "house-of-cards" structure, influencing fluid flow and ability to print and reform structures. Laponite XLG addition to PEG reduced the flow behavior index and reduced the recovery time of solutions from infinite (Newtonian fluid) to seconds which is more appropriate for bioprinting applications. The rheological behavior of the nanocomposite hydrogels was found to be dominated by the behavior of Laponite network, independent of PEG addition. Recovery time of nanocomposite hydrogels was controlled by the PEG:Laponite ratio and ability of Laponite XLG to interact with itself to form a "house-of-cards" structure. Rapid adsorption or excess of PEG prohibits necessary charge−charge interactions between Laponite particles; concentrations of Laponite below 4% wt/vol with 10% wt./vol PEG (3.4 kDa) are unable to recover quickly. For practical applications, electrostatic repulsion and van der Waals attractive forces must be balanced. PEG presents a special situation due to the extensive literature available supporting strong interactions between Laponite and polymer. The present study combines rheological properties with application to show that appropriate concentrations of PEG/Laponite suspensions can be used as an appropriate bioink. While this work gives unique insight into the macroscopic use of PEG/Laponite as a bioink, structural information is obtained from previous work by others.[11,20,22,61−63] We believe the present study complements both colloidal literature and biomedical literature in balancing colloidal forces and methods of study with appropriate cellular assays to optimize bioinks. We have proposed linear PEG/Laponite interactions and subsequent rheological profile for bioink characterization to determine critical parameters necessary for bioinks before more complicated systems are developed.

ASSOCIATED CONTENT

Supporting Information

The Supporting Information is available free of charge on the ACS Publications website at DOI: 10.1021/acs.langmuir.7b02540.

Print extrusion graph and recovery time graph of PEG/Laponite formulations. Cell Tracker images of PEG and PBS prints. Live/Dead images of extruded cells. (PDF)

AUTHOR INFORMATION

Corresponding Author

*E-mail: gaharwar@tamu.edu. Tel. 979-458-5540. Fax. 979-845-4450.

ORCID

Akhilesh K. Gaharwar: 0000-0002-0284-0201

Author Contributions

The manuscript was written with contributions made by all authors. All authors have given approval to the final version of the manuscript.

Notes

The authors declare no competing financial interest.

ACKNOWLEDGMENTS

A.K.G. would like to acknowledge financial support from the National Science Foundation (CBET 1705852), and the

DOI: 10.1021/acs.langmuir.7b02540
Langmuir 2018, 34, 917−925

National Institute of Health (DP2 EB026265, R03 EB023454). C.W.P. would like to acknowledge Mu'ath Adlouni, Jefferey Chen, Samantha Sliva, Christian Bergh, and Seok Young "Jenny" Hong for rheology and printing work.

REFERENCES

(1) Schexnailder, P.; Loizou, E.; Porcar, L.; Butler, P.; Schmidt, G. Heterogeneity in nanocomposite hydrogels from poly(ethylene oxide) cross-linked with silicate nanoparticles. *Phys. Chem. Chem. Phys.* **2009**, *11* (15), 2760−2766.
(2) Chimene, D.; Alge, D. L.; Gaharwar, A. K. Two-Dimensional Nanomaterials for Biomedical Applications: Emerging Trends and Future Prospects. *Adv. Mater.* **2015**, *27* (45), 7261−7284.
(3) Gaharwar, A. K.; Peppas, N. A.; Khademhosseini, A. Nanocomposite hydrogels for biomedical applications. *Biotechnol. Bioeng.* **2014**, *111* (3), 441−453.
(4) Paineau, E.; Bihannic, I.; Baravian, C.; Philippe, A.-M.; Davidson, P.; Levitz, P.; Funari, S. S.; Rochas, C.; Michot, L. J. Aqueous Suspensions of Natural Swelling Clay Minerals. 1. Structure and Electrostatic Interactions. *Langmuir* **2011**, *27* (9), 5562−5573.
(5) Ruzicka, B.; Zaccarelli, E. A fresh look at the Laponite phase diagram. *Soft Matter* **2011**, *7* (4), 1268−1286.
(6) Mourchid, A.; Delville, A.; Lambard, J.; Lecolier, E.; Levitz, P. Phase Diagram of Colloidal Dispersions of Anisotropic Charged-Particles - Equilibrium Properties, Structure, and Rheology of Laponite Suspensions. *Langmuir* **1995**, *11* (6), 1942−1950.
(7) Levitz, P.; Lecolier, E.; Mourchid, A.; Delville, A.; Lyonnard, S. Liquid-solid transition of Laponite suspensions at very low ionic strength: Long-range electrostatic stabilisation of anisotropic colloids. *Europhys. Lett.* **2000**, *49* (5), 672−677.
(8) Avery, R. G.; Ramsay, J. D. F. Colloidal Properties of Synthetic Hectorite Clay Dispersions 2: Light and Small-Angle Neutron-Scattering. *J. Colloid Interface Sci.* **1986**, *109* (2), 448−454.
(9) Rosta, L.; Vongunten, H. R. Light-Scattering Characterization of Laponite Sols. *J. Colloid Interface Sci.* **1990**, *134* (2), 397−406.
(10) Mori, Y.; Togashi, K.; Nakamura, K. Colloidal properties of synthetic hectorite clay dispersion measured by dynamic light scattering and small angle X-ray scattering. *Adv. Powder Technol.* **2001**, *12* (1), 45−59.
(11) Nelson, A.; Cosgrove, T. Dynamic light scattering studies of poly(ethylene oxide) adsorbed on laponite: Layer conformation and its effect on particle stability. *Langmuir* **2004**, *20* (24), 10382−10388.
(12) Pawar, N.; Bohidar, H. B. Surface selective binding of nanoclay particles to polyampholyte protein chains. *J. Chem. Phys.* **2009**, *131* (4), 045103.
(13) Thakur, A.; Jaiswal, M. K.; Peak, C. W.; Carrow, J. K.; Gentry, J.; Dolatshahi-Pirouz, A.; Gaharwar, A. K. Injectable shear-thinning nanoengineered hydrogels for stem cell delivery. *Nanoscale* **2016**, *8* (24), 12362−12372.
(14) Nelson, A.; Cosgrove, T. Small-angle neutron scattering study of adsorbed pluronic tri-block copolymers on laponite. *Langmuir* **2005**, *21* (20), 9176−9182.
(15) Wu, C. J.; Gaharwar, A. K.; Chan, B. K.; Schmidt, G. Mechanically Tough Pluronic F127/Laponite Nanocomposite Hydrogels from Covalently and Physically Cross-Linked Networks. *Macromolecules* **2011**, *44* (20), 8215−8224.
(16) Boucenna, I.; Royon, L.; Colinart, P.; Guedeau-Boudeville, M. A.; Mourchid, A. Structure and Thermorheology of Concentrated Pluronic Copolymer Micelles in the Presence of Laponite Particles. *Langmuir* **2010**, *26* (18), 14430−14436.
(17) Haraguchi, K.; Xu, Y. J. Thermal analyses of poly(N-isopropylacrylamide) in aqueous solutions and in nanocomposite gels. *Colloid Polym. Sci.* **2012**, *290* (16), 1627−1636.
(18) Haraguchi, K.; Xu, Y. J.; Li, G. Molecular Characteristics of Poly(N-isopropylacrylamide) Separated from Nanocomposite Gels by Removal of Clay from the Polymer/Clay Network. *Macromol. Rapid Commun.* **2010**, *31* (8), 718−723.
(19) Haraguchi, K.; Li, H. J.; Song, L. Ultra-high hydrophobicity on the surface of nanocomposite hydrogels with a poly(n-isopropylacrylamide)/clay network. *J. Colloid Interface Sci.* **2008**, *326*, 41−50.
(20) Schmidt, G.; Nakatani, A. I.; Han, C. C. Rheology and flow-birefringence from viscoelastic polymer-clay solutions. *Rheol. Acta* **2002**, *41* (1−2), 45−54.
(21) Schmidt, G.; Nakatani, A. I.; Butler, P. D.; Han, C. C. Small-angle neutron scattering from viscoelastic polymer-clay solutions. *Macromolecules* **2002**, *35* (12), 4725−4732.
(22) Nelson, A.; Cosgrove, T. A small-angle neutron scattering study of adsorbed poly(ethylene oxide) on laponite. *Langmuir* **2004**, *20* (6), 2298−2304.
(23) Gaharwar, A. K.; Schexnailder, P. J.; Dundigalla, A.; White, J. D.; Matos-Perez, C. R.; Cloud, J. L.; Seifert, S.; Wilker, J. J.; Schmidt, G. Highly Extensible Bio-Nanocomposite Fibers. *Macromol. Rapid Commun.* **2011**, *32* (1), 50−57.
(24) Ruzicka, B.; Zaccarelli, E.; Zulian, L.; Angelini, R.; Sztucki, M.; Moussaïd, A.; Narayanan, T.; Sciortino, F. Observation of empty liquids and equilibrium gels in a colloidal clay. *Nat. Mater.* **2011**, *10* (1), 56−60.
(25) Mourchid, A.; Delville, A.; Lambard, J.; LeColier, E.; Levitz, P. Phase Diagram of Colloidal Dispersions of Anisotropic Charged Particles: Equilibrium Properties, Structure, and Rheology of Laponite Suspensions. *Langmuir* **1995**, *11* (6), 1942−1950.
(26) Mourchid, A.; Delville, A.; Levitz, P. Sol−gel transition of colloidal suspensions of anisotropic particles of laponite. *Faraday Discuss.* **1995**, *101*, 275−285.
(27) Lorthioir, C.; Khalil, M.; Wintgens, V.; Amiel, C. Segmental Motions of Poly(ethylene glycol) Chains Adsorbed on Laponite Platelets in Clay-Based Hydrogels: A-NMR Investigation. *Langmuir* **2012**, *28* (20), 7859−7871.
(28) Zhang, J. X.; Feng, X.; Patil, H.; Tiwari, R. V.; Repka, M. A. Coupling 3D printing with hot-melt extrusion to produce controlled-release tablets. *Int. J. Pharm.* **2017**, *519* (1−2), 186−197.
(29) Youssef, A.; Hollister, S. J.; Dalton, P. D. Additive manufacturing of polymer melts for implantable medical devices and scaffolds. *Biofabrication* **2017**, *9* (1), 012002.
(30) Yang, C. C.; Tian, X. Y.; Liu, T. F.; Cao, Y.; Li, D. C. 3D printing for continuous fiber reinforced thermoplastic composites: mechanism and performance. *Rapid Prototyping Journal* **2017**, *23* (1), 209−215.
(31) Chimene, D.; Lennox, K. K.; Kaunas, R. R.; Gaharwar, A. K. Advanced Bioinks for 3D Printing: A Materials Science Perspective. *Ann. Biomed. Eng.* **2016**, *44* (6), 2090−2102.
(32) Sommer, M. R.; Alison, L.; Minas, C.; Tervoort, E.; Ruhs, P. A.; Studart, A. R. 3D printing of concentrated emulsions into multiphase biocompatible soft materials. *Soft Matter* **2017**, *13* (9), 1794−1803.
(33) Xavier, J. R.; Thakur, T.; Desai, P.; Jaiswal, M. K.; Sears, N.; Cosgriff-Hernandez, E.; Kaunas, R.; Gaharwar, A. K. Bioactive Nanoengineered Hydrogels for Bone Tissue Engineering: A Growth-Factor-Free Approach. *ACS Nano* **2015**, *9* (3), 3109−3118.
(34) Nojoomi, A.; Tamjid, E.; Simchi, A.; Bonakdar, S.; Stroeve, P. Injectable polyethylene glycol-laponite composite hydrogels as articular cartilage scaffolds with superior mechanical and rheological properties. *Int. J. Polym. Mater.* **2017**, *66* (3), 105−114.
(35) Davila, J. L.; d'Avila, M. A. Laponite as a rheology modifier of alginate solutions: Physical gelation and aging evolution. *Carbohydr. Polym.* **2017**, *157*, 1−8.
(36) Gaharwar, A. K.; Avery, R. K.; Assmann, A.; Paul, A.; McKinley, G. H.; Khademhosseini, A.; Olsen, B. D. Shear-Thinning Nanocomposite Hydrogels for the Treatment of Hemorrhage. *ACS Nano* **2014**, *8* (10), 9833−9842.
(37) Gaharwar, A. K.; Dammu, S. A.; Canter, J. M.; Wu, C. J.; Schmidt, G. Highly Extensible, Tough, and Elastomeric Nanocomposite Hydrogels from Poly(ethylene glycol) and Hydroxyapatite Nanoparticles. *Biomacromolecules* **2011**, *12* (5), 1641−1650.
(38) Nicolai, T.; Cocard, S. Light scattering study of the dispersion of laponite. *Langmuir* **2000**, *16* (21), 8189−8193.

DOI: 10.1021/acs.langmuir.7b02540
Langmuir 2018, 34, 917−925

(39) Shahin, A.; Joshi, Y. M. Hyper-Aging Dynamics of Nanoclay Suspension. *Langmuir* **2012**, *28* (13), 5826−5833.
(40) Rand, B.; Melton, I. E. Particle interactions in aqueous kaolinite suspensions. *J. Colloid Interface Sci.* **1977**, *60* (2), 308−320.
(41) Gibaud, T.; Barentin, C.; Taberlet, N.; Manneville, S. Shear-induced fragmentation of laponite suspensions. *Soft Matter* **2009**, *5* (16), 3026−3037.
(42) Kurokawa, A.; Vidal, V.; Kurita, K.; Divoux, T.; Manneville, S. Avalanche-like fluidization of a non-Brownian particle gel. *Soft Matter* **2015**, *11* (46), 9026−9037.
(43) Martin, J. D.; Thomas Hu, Y. Transient and steady-state shear banding in aging soft glassy materials. *Soft Matter* **2012**, *8* (26), 6940−6949.
(44) Aguado, B. A.; Mulyasasmita, W.; Su, J.; Lampe, K. J.; Heilshorn, S. C. Improving Viability of Stem Cells During Syringe Needle Flow Through the Design of Hydrogel Cell Carriers. *Tissue Eng., Part A* **2012**, *18* (7−8), 806−815.
(45) Truby, R. L.; Lewis, J. A. Printing soft matter in three dimensions. *Nature* **2016**, *540* (7633), 371−378.
(46) Malkin, A. Y.; Isayev, A. I. *Rheology - Concepts, Methods, and Applications* (2nd ed.); ChemTec Publishing.
(47) McFarlane, N. L.; Wagner, N. J.; Kaler, E. W.; Lynch, M. L. Poly(ethylene oxide) (PEO) and Poly(vinyl pyrolidone) (PVP) Induce Different Changes in the Colloid Stability of Nanoparticles. *Langmuir* **2010**, *26* (17), 13823−13830.
(48) Chiu, Y. L.; Chen, S. C.; Su, C. J.; Hsiao, C. W.; Chen, Y. M.; Chen, H. L.; Sung, H. W. pH-triggered injectable hydrogels prepared from aqueous N-palmitoyl chitosan: In vitro characteristics and in vivo biocompatibility. *Biomaterials* **2009**, *30* (28), 4877−4888.
(49) Roux, R.; Ladaviere, C.; Montembault, A.; David, L.; Delair, T. Shear Thinning Three-Dimensional Colloidal Assemblies of Chitosan and Poly(lactic acid) Nanoparticles. *J. Phys. Chem. B* **2013**, *117* (24), 7455−7464.
(50) Lindsey, S.; Piatt, J. H.; Worthington, P.; Sonmez, C.; Satheye, S.; Schneider, J. P.; Pochan, D. J.; Langhans, S. A. Beta Hairpin Peptide Hydrogels as an Injectable Solid Vehicle for Neurotrophic Growth Factor Delivery. *Biomacromolecules* **2015**, *16* (9), 2672−2683.
(51) Dong, Y. Z.; Wang, W. H.; Veiseh, O.; Appel, E. A.; Xue, K.; Webber, M. J.; Tang, B. C.; Yang, X. W.; Weir, G. C.; Langer, R.; Anderson, D. G. Injectable and Glucose-Responsive Hydrogels Based on Boronic Acid-Glucose Complexation. *Langmuir* **2016**, *32* (34), 8743−8747.
(52) Gaharwar, A. K.; Schexnailder, P.; Kaul, V.; Akkus, O.; Zakharov, D.; Seifert, S.; Schmidt, G. Highly Extensible Bio-Nanocomposite Films with Direction-Dependent Properties. *Adv. Funct. Mater.* **2010**, *20* (3), 429−436.
(53) Schexnailder, P. J.; Gaharwar, A. K.; Bartlett, R. L.; Seal, B. L.; Schmidt, G. Tuning Cell Adhesion by Incorporation of Charged Silicate Nanoparticles as Cross-Linkers to Polyethylene Oxide. *Macromol. Biosci.* **2010**, *10* (12), 1416−1423.
(54) Gaharwar, A. K.; Rivera, C. P.; Wu, C. J.; Schmidt, G. Transparent, elastomeric and tough hydrogels from poly(ethylene glycol) and silicate nanoparticles. *Acta Biomater.* **2011**, *7* (12), 4139−4148.
(55) Gaharwar, A. K.; Schexnailder, P. J.; Kline, B. P.; Schmidt, G. Assessment of using Laponite (R) cross-linked poly(ethylene oxide) for controlled cell adhesion and mineralization. *Acta Biomater.* **2011**, *7* (2), 568−577.
(56) Burdick, J. A.; Anseth, K. S. Photoencapsulation of osteoblasts in injectable RGD-modified PEG hydrogels for bone tissue engineering. *Biomaterials* **2002**, *23* (22), 4315−4323.
(57) Bryant, S. J.; Anseth, K. S.; Lee, D. A.; Bader, D. L. Crosslinking density influences the morphology of chondrocytes photoencapsulated in PEG hydrogels during the application of compressive strain. *J. Orthop. Res.* **2004**, *22* (5), 1143−1149.
(58) Moon, J. J.; Saik, J. E.; Poché, R. A.; Leslie-Barbick, J. E.; Lee, S.-H.; Smith, A. A.; Dickinson, M. E.; West, J. L. Biomimetic hydrogels with pro-angiogenic properties. *Biomaterials* **2010**, *31* (14), 3840−3847.
(59) Weber, L. M.; He, J.; Bradley, B.; Haskins, K.; Anseth, K. S. PEG-based hydrogels as an in vitro encapsulation platform for testing controlled β-cell microenvironments. *Acta Biomater.* **2006**, *2* (1), 1−8.
(60) Compton, B. G.; Lewis, J. A. 3D-Printing of Lightweight Cellular Composites. *Adv. Mater.* **2014**, *26* (34), 5930−5935.
(61) Mohanty, R. P.; Suman, K.; Joshi, Y. M. In situ ion induced gelation of colloidal dispersion of Laponite: Relating microscopic interactions to macroscopic behavior. *Appl. Clay Sci.* **2017**, *138*, 17−24.
(62) Zulian, L.; Ruzicka, B.; Ruocco, G. Influence of an adsorbing polymer on the aging dynamics of Laponite clay suspensions. *Philos. Mag.* **2008**, *88* (33−35), 4213−4221.
(63) Zulian, L.; Marques, F. A. D.; Emilitri, E.; Ruocco, G.; Ruzicka, B. Dual aging behaviour in a clay-polymer dispersion. *Soft Matter* **2014**, *10* (25), 4513−4521.

DOI: 10.1021/acs.langmuir.7b02540
Langmuir 2018, 34, 917−925